Structure 14, 1587–1597, October 2006 ©2006 Elsevier Ltd All rights reserved DOI 10.1016/j.str.2006.08.008

Structure of Complement Component C2a: Implications for Convertase Formation and Substrate Binding

Fin J. Milder,[1] Hans C.A. Raaijmakers,[1,4] Mitja D.A.A. Vandeputte,[1,5] Arie Schouten,[1] Eric G. Huizinga,[1] Roland A. Romijn,[2] Wieger Hemrika,[2] Anja Roos,[3] Mohamed R. Daha,[3] and Piet Gros[1,*]

[1] Crystal and Structural Chemistry
Bijvoet Center for Biomolecular Research
Faculty of Science
[2] ABC Expression Center
Utrecht University
3584 CH Utrecht
The Netherlands
[3] Department of Nephrology
Leiden University Medical Center
2300 RC Leiden
The Netherlands

Summary

C2a provides the catalytic center to the convertase complexes of the classical and lectin-binding pathways of complement activation. We determined two crystal structures of full-length C2a, with and without a pseudo ligand bound. Both structures reveal a near-active conformation of the catalytic center of the serine protease domains, while the von Willebrand factor A-type domains display an intermediate activation state of helix α7 with an open, activated metal-ion-dependent adhesion site. The open adhesion site likely serves to enhance the affinity for the ligand C4b, similar to "inside-out" signaling in integrins. Surprisingly, the N-terminal residues of C2a are buried in a crevice near helix α7, indicative of a structural switch between C2 and C2a. Extended loops on the protease domain possibly envelop the protruding anaphylatoxin domain of the substrate C3. Together with a putative substrate-induced completion of the oxyanion hole, this may contribute to the high substrate specificity of the convertases.

Introduction

The complement system plays a crucial role in mammalian immune defense (for review, see, e.g., Walport, 2001a, 2001b). It consists of over 30 fluid-phase and cell-surface proteins that recognize and kill invading pathogens, present them to the adaptive immune system, and elicit inflammatory responses. Three pathways activate the complement system: the classical, the lectin, and the alternative pathway. Complement protein C2 is critical to the classical and lectin pathways because it provides the proteolytic center to their C3 and C5 convertases, which proteolytically activate C3 and C5, enabling amplification of the complement response, stimulation of inflammatory responses, opsonization of pathogenic particles, and initiation of the terminal membrane-attack phase of the complement.

Human C2 (732 amino acid residues, molecular weight of 100 kDa) is produced as an inactive, heavily glycosylated zymogen consisting of five domains: three N-terminal complement-control-protein (CCP) domains, a von Willebrand factor A-type (VWA) domain, and a C-terminal trypsin-like serine proteinase (SP) domain (Bentley, 1986) (see Figure 1A). The last two domains, VWA and SP, form the C2a fragment (residues 224–732, 70 kDa) that is produced in the proteolytic activation cascade of the classical and lectin pathways. Activation starts by binding of the zymogen C2 in a magnesium-dependent manner to activated pathogen-bound complement component C4b (193 kDa). Proteolysis at Arg-223–Lys-224, by either C1s of the classical pathway or MASP2 of the lectin pathway, yields a complex of C4b and C2a. This complex is referred to as C4b2a and is the active C3 convertase of the classical and lectin pathways. The C3 convertase is instable and dissociates with a half-life time of 60 s (Kerr, 1980). Once dissociated, C2a loses proteolytic activity and cannot reassociate with C4b (Kerr and Parkes, 1984). C2 and C2a are homologous to factor B and its fragment Bb of the alternative pathway (39% sequence identity between full-length proteins as well as protein fragments). Factor B associates with complement component C3b and after proteolysis yields the C3 convertase of the alternative pathway, C3bBb, which has a half-life time of 90 s (Pangburn and Muller-Eberhard, 1986). The C3 convertases, C4b2a and C3bBb, cleave C3 into the anaphylatoxin C3a and C3b. Attachment of C3b to either C4b2a or C3bBb yields the C5 convertases, C4b2a3b and $C3b_2Bb$, respectively, that cleave complement component C5 (reviewed by Rawal and Pangburn, 2001).

C2 and factor B differ from chymotrypsinogens and trypsinogens in their mechanism of activation. In chymotrypsinogens and trypsinogens, cleavage in the N terminus generates a new N terminus (Ile-16 in trypsin) that induces formation of the oxyanion hole (Bode, 1979; Khan and James, 1998). In C2 and factor B, instead, proteolysis occurs between the third CCP and the VWA domain, leaving the VWA domain attached to the N terminus of the SP domain after activation; thus, no new N terminus in the SP domain is provided that may induce oxyanion-hole formation. The VWA domain is homologous to integrin-inserted (I) domains and contains a metal-ion-dependent adhesion site (MIDAS) motif. Amino acid residue mutations in the MIDAS motif abolish hemolytic activity (Horiuchi et al., 1991), indicating a critical role for the MIDAS motif in convertase formation, stability, or activity. It was hypothesized that the VWA domain might play an activating role via a conformational change similar to that observed in I domains of integrins in outside-in signaling (Bhattacharya et al., 2004), where ligand binding at the MIDAS site induces

*Correspondence: p.gros@chem.uu.nl
[4] Present address: N.V. Organon, Molecular Design & Informatics, Molenstraat 110, 5342 CC Oss, The Netherlands.
[5] Present address: Department of Neuroscience, Erasmus Medical Center, 3000 DR, Rotterdam, The Netherlands.

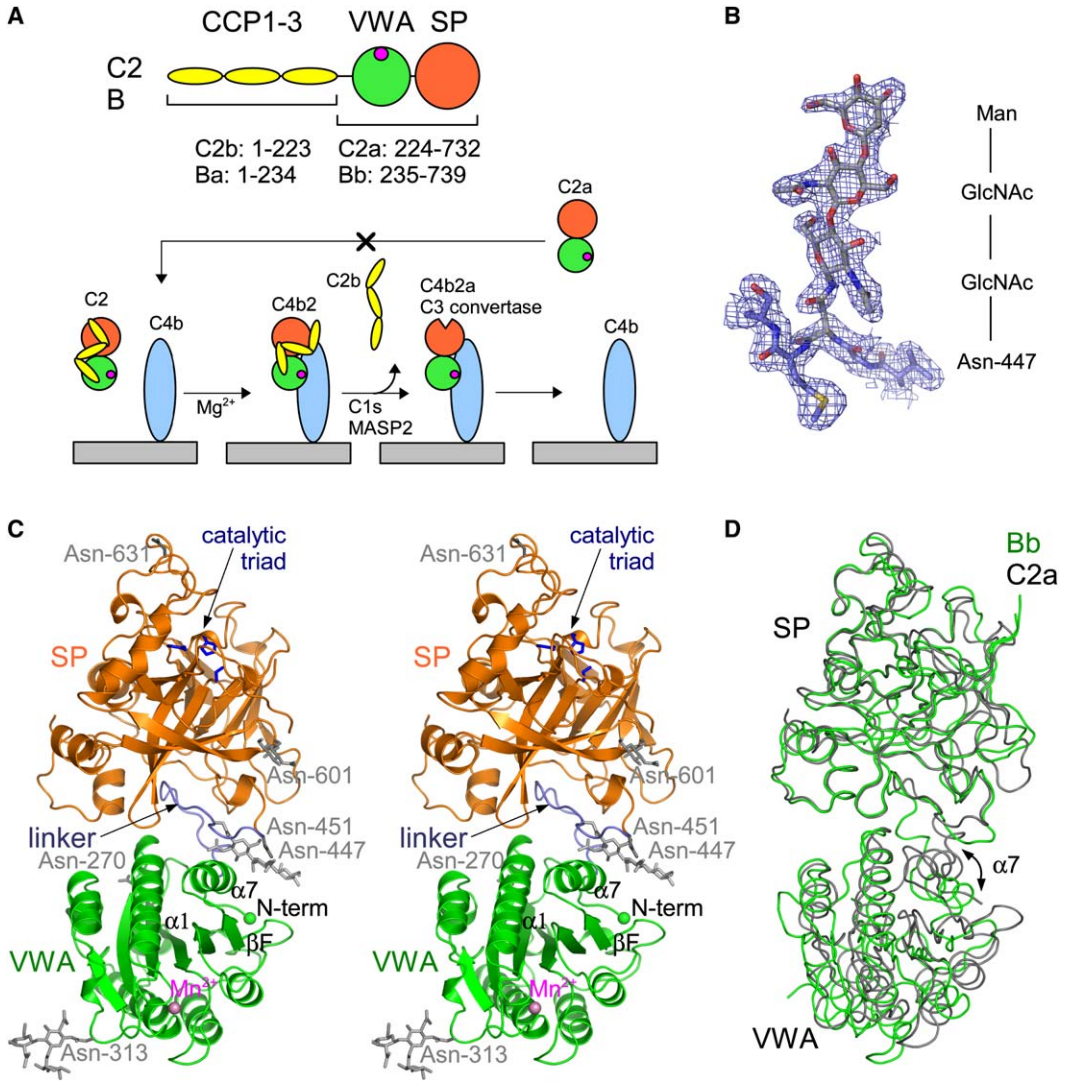

Figure 1. Crystal Structure of C2a

(A) Schematic representation of domain topology of C2 and formation of the C3 convertase.

(B) Electron density ($2mF_o - DF_c$, φ_c) of the glycan attached to Asn-447; Asn-447-GlcNac-GlcNac-Man are shown.

(C) Stereo ribbon representation of the C2a-Mn^{2+} structure; the catalytic triad (blue) in the SP domain (orange), the linker region (light blue) between the SP and VWA domains (green; its N-terminal residue is indicated by a green sphere), the manganese ion (pink) bound at the MIDAS motif, and the six glycosylation sites (gray) are shown.

(D) Overlay of C2a (black) and Bb (1rrk, green) (Ponnuraj et al., 2004) superimposed on the SP domains; the different positions of the α7 helix in the VWA domains are indicated.

a ~10 Å movement of the C-terminal α7 helix (Emsley et al., 1997, 2000). In analogy to disulphide-bridge engineered I domains, Ponnuraj et al. (2004) made a Bb disulphide mutant (Cys-428–Cys-435) enforcing the VWA domain in an artificial active conformation in the absence of ligand C3b. The structure of this engineered Bb, which was also truncated at the N terminus by 7 residues, showed that the SP domain displays an active conformation of the catalytic Asp-His-Ser triad and a near-active conformation of the oxyanion hole, i.e., loop 670–674 adopts a conformation similar to that of mature chymotrypsins and trypsins, except that peptide bond 671–672 is flipped by ~180° (Ponnuraj et al., 2004). In this conformation, the negative charge of the oxyanion intermediate cannot be stabilized. The structure of Bb covalently inhibited by di-isopropyl phosphate has this peptide plane in the active orientation, indicating that a fully active site may be induced by substrate binding (Ponnuraj et al., 2004). The role of VWA, however, in the molecular mechanisms of convertase formation, stability, or activity remains unclear.

We have expressed human C2 and C2a in mammalian cells, crystallized C2a, and tested C2 and two C2 glycan-deletion mutants in hemolytic assays. Here, we present crystal structures of native, glycosylated C2a, one unliganded and one with a pseudo ligand bound to the VWA domain. The N-terminal residues, absent in the truncated Bb fragment (Ponnuraj et al., 2004), play an important structural role. They interact with the C-terminal tail of VWA and partake in the VWA-SP interface. Comparison of the SP domains of C2a and Bb indicates

a distinct binding groove for the scissile loop of C3. Placing the C3 structure (Janssen et al., 2005) onto the SP domains indicates putative interaction sites in the proteinase-substrate complex.

Results and Discussion

Expression, Purification, and Activity of Recombinant C2, C2a, and C2 Mutants

Human C2a (residues 224–732) with an N-terminal His_6-tag was stably expressed in baby-hamster kidney (BHK) cells. Stable BHK-cell lines secreted 10–15 mg C2a per liter medium. Purification yielded 10 mg C2a per liter medium. Purified C2a runs as a single band on SDS-PAGE at 70 kDa. The observed molecular weight is in agreement with the extent (10–15 w/w %) of glycosylation observed in human plasma (Tomana et al., 1985). Human C2 (residues 1–732) and two C2 single-glycan-deletion mutants (N447D and N451D) and one C2 double-glycan-deletion mutant (N447D/N451D) were transiently expressed in human embryonic kidney (HEK293E) cells. Native and mutant C2 gave comparable expression levels of 15–20 mg protein per liter medium. The harvested media from BHK and HEK293E cells were tested for complement activity in a hemolytic assay by using sensitized sheep erythrocytes. Recombinant C2 in medium showed a hemolytic activity (normalized for concentration) that was comparable (98% ± 31%) to native C2 in normal human serum. No hemolytic activity for the harvested C2a-containing medium was observed. This is in agreement with the observation that C2, and not C2a, associates with C4b to form an active convertase (Kerr, 1980).

Structure Determinations

Crystals of C2a were obtained by the hanging-drop vapor-diffusion method. C2a was crystallized with 35% w/v polyethylene glycol 1000 (PEG-1000) and 0.1 M malonate-imidazol boric acid buffer (MIB-buffer) at pH 7.0. One crystal was grown in the presence of 20 mM LiCl and diffracted to a resolution of 2.7 Å. A second crystal was grown in the presence of 3% w/v xylitol. We soaked this crystal in a solution containing 10 mM $MnCl_2$. This crystal diffracted to a resolution of 2.1 Å. We refer to the two diffraction data sets and structures as C2a-Li^+ (C2a in the presence of LiCl) and C2a-Mn^{2+} (C2a soaked in $MnCl_2$), respectively. Data collection and processing statistics for both crystals are given in Table 1.

First, we determined the structure of C2a-Li^+. For molecular replacement, we used the structures of the isolated VWA (Protein Data Bank entry 1q0p) and SP (1dle) domains of factor B as search models (Bhattacharya et al., 2004; Jing et al., 2000). The structures of Bb (Ponnuraj et al., 2004) containing both the VWA and the SP domain were not made available at that moment. A clear and correct solution in molecular replacement was obtained when using the program Phaser (Storoni et al., 2004). The model was rebuilt by using the graphics program O (Jones et al., 1991) and was refined by using programs CNS (Brunger et al., 1998) and REFMAC (CCP4, 1994; Murshudov et al., 1997). Electron density allowed modeling of the vector-derived N-terminal Ser; C2a residues 224–732 (except for residues 395–397, 408–413, and 691–694); partial glycans at Asn-270, Asn-313, Asn-447, Asn-451, and Asn-601; and 38 water molecules. No additional density was observed at the putative glycosylation site Asn-631. The final model had an R factor and an R_{free} of 21.2% and 28.7%, respectively, and displayed good stereochemistry. Statistics on the model quality are given in Table 1.

Table 1. Crystallographic Data Collection and Refinement Statistics

	C2a-Li^+	C2a-Mn^{2+}
Data Collection Statistics		
Space group	$P2_1$	$P2_1$
Cell dimensions	a = 51.16 Å	a = 51.48 Å
	b = 75.08	b = 77.19
	c = 71.56	c = 70.86
	β = 110.32°	β = 109.55°
Resolution (Å)	37.5–2.7	50.5–2.1
Completeness (%)	98.5	89.9
Multiplicity	3.6 (3.2)	3.6 (2.9)
R_{merge} (%)	8.5 (42)	6.1 (52)
I/σI	13.7 (2.4)	15.1 (1.9)
Refinement Statistics		
Number of reflections (work/test)	13,177/690	26,081/1,389
R/R_{free} (%)	21.2/28.7	18.9/24.0
B factor (Å^2)	32.1	22.5
Rmsd bond length (Å)	0.004	0.003
Rmsd bond angle (°)	0.674	0.862
Number of protein atoms	3,928	3,994
Number of glycan atoms	144	91
Number of water molecules	38	133
Number of ions	—	1 (Mn^{2+})
Number of ligand atoms	—	7 (malonate)

Values in parentheses refer to a high-resolution shell.

Second, we determined the structure of C2a-Mn^{2+} by molecular replacement with the structure of C2a-Li^+. The complete model of C2a-Li^+ was placed in the unit cell, and the position of the domains was optimized by rigid-body refinement with Phaser. Model building and refinement yielded a final model consisting of the vector-derived Ser residue; C2a residues 224–732, except loop 687–693; partial glycans at Asn-313, Asn-447, and Asn-601; and 133 water molecules. Even though the C2a-Mn^{2+} crystal diffracted to higher resolution than C2a-Li^+, less electron density was visible at the glycosylation sites. The final model had an R factor and an R_{free} of 18.9% and 24.0% and good stereochemistry (see Table 1). An example of electron density is shown in Figure 1B.

The model of C2a-Mn^{2+} was used to finalize the modeling of C2a-Li^+. In the original C2a-Li^+ model, VWA helix α6 (residues 398–407) was missing. Density at the 0.5σ contour level correlated very well with the superimposed C2a-Mn^{2+} structure in this region; therefore, this helix was included in the model. As a consequence, the R factor and R_{free} dropped from 21.7%/29.1% to 21.2%/28.7%. Continuous electron density was visible throughout the α6 helix at 0.8σ and for the main chain of residues 401–406 at the 1σ contour level. The final position of the helix in the C2a-Li^+ model is very similar to that in C2a-Mn^{2+}. SP loop 687–694 is most likely disordered in both crystals. For C2a-Li^+ and C2a-Mn^{2+}, 4 and 7 residues, respectively, of this loop were not modeled. The

two models, C2a-Li^+ and C2a-Mn^{2+}, differ 8° in domain-domain orientation, which is possibly due to small differences in crystallization conditions and soaking of the C2a-Mn^{2+} crystal. The separate VWA and SP domains show root-mean-square coordinate differences of 0.54 and 0.59 Å, respectively, for all Cα positions.

For C2a-Mn^{2+}, we observed a significant (12σ) electron-density peak at the ion binding position in the MIDAS site. We modeled a manganese ion at this position. The Mn^{2+} ion displays an octahedral coordination provided by MIDAS residues Ser-240, Ser-242, and Thr-317, two water molecules, and one malonate molecule, originating from the crystallization buffer and acting as a pseudo ligand. In the case of C2a-Li^+, no significant electron-density peak was present at the ion binding site, nor was density present for a pseudo ligand. Possibly, the ion-binding site was occupied by the weakly scattering Li^+ ion. However, the resolution (2.7 Å) of the diffraction data does not allow for modeling of Li^+ binding, and no ion was included at the MIDAS site for C2a-Li^+.

Overall Structure of C2a

The overall structure of C2a is characterized by the VWA and SP domains that are in close contact (see Figure 1C). The overall fold of C2a is similar to that of its homolog, Bb (Ponnuraj et al., 2004), but significant differences are apparent between the structures. In part, this is expected given the amino acid sequence identity of 39% and the differences in glycosylation. C2a has six whereas Bb has two putative N-linked glycosylation sites. The orientation of the VWA-SP domains in C2a-Li^+ and C2a-Mn^{2+} differ by 16.5° and 21.5°, respectively, from the orientation observed in Bb (see Figure 1D). The VWA-SP orientation differs by only 8° between C2a-Li^+ and C2a-Mn^{2+}. In part, these different domain-domain orientations in C2a and Bb may be due to crystal packing effects and may reflect flexibility in the domain-domain linkage. However, as we will argue below, differences in glycosylation, the introduced disulphide bridge in Bb, and, in particular, the N-terminal truncation in Bb affect the interface region. The absence of mutations and truncations in C2a allows for the analysis of the unperturbed state of the MIDAS motif, the α7 helix of VWA, and the VWA-SP interface.

MIDAS Motif

The MIDAS site in C2a is formed by Asp-240, Ser-242, and Ser-244 from loop βAα1; Thr-317 from loop α3α4; and Asp-356 from loop βDα5 (Figure 2A). In C2a-Li^+, no ligand is bound and no ion can be observed, whereas a metal ion and pseudo ligand are clearly bound to the MIDAS motif in C2a-Mn^{2+}. Putatively, the pseudo ligand, malonate, originating from the crystallization buffer, binds in a similar way as the carboxylate moiety of an aspartate or glutamate residue of the true ligand, C4b. In C2a-Mn^{2+}, the manganese ion is coordinated by hydroxyl groups from residues Ser-242, Ser-244, and Thr-317 and two waters, one of which mediates contacts with the two MIDAS aspartatic acids 240 and 356. The octahedral coordination is completed by a carboxylate oxygen of the pseudo ligand, malonate (Figure 2A). This conformation of the MIDAS residues is virtually identical to that observed in the engineered Bb structure and other open and ligand-bound MIDAS sites (Emsley et al., 1997, 2000; Shimaoka et al., 2003) (see Figure 2A). Superposition of the MIDAS sites of C2a-Li^+ and C2a-Mn^{2+} shows that the side chain of Ser-244 in C2a-Li^+ is rotated by ~90° and thus points its hydroxyl away from the metal-binding site and forms a hydrogen bond with the carboxylate group of Asp-356 (Figure 2A). All other residues in the MIDAS site show identical conformations in C2a-Li^+ and C2a-Mn^{2+}. The minor rearrangement of Ser-244 may compensate for the loss of either a +1 or +2 charge when either a Li^+ ion or a water molecule, respectively, replaces Mn^{2+}. In contrast, in an ion-free and unliganded disulphide engineered α_L I domain Asp-239 (equivalent to Asp-356 in C2a) rotates away and hence compensates for the loss of a +2 charge (Shimaoka et al., 2003). Most surprisingly, the liganded C2a-Mn^{2+} and unliganded C2a-Li^+ structures display essentially identical, both open, MIDAS motifs. Thus, the open conformation of the MIDAS site in C2a occurs independently of ligand binding.

VWA α7 Helix

In integrin-I domains, ligand binding at the MIDAS site is coupled to a 10 Å displacement of the C-terminal α7 helix from an inactive, closed conformation to one that is activated and open (Emsley et al., 1997, 2000). Concerted movements of loop βAα1 and helix α1 and the subsequent rearrangement of loops βDα5 and βEα6 transmit the signal from the MIDAS site to loop βFα7 and helix α7. The conformation of these loops and helices is identical in the unliganded and pseudo liganded C2a structures. Comparison of C2a with engineered, open Bb shows that loops βAα1 and βDα5 and helix α1 have similar conformations in the two structures (Figure 2B). Their conformation corresponds best to the open conformation of these loops and helix in α I domains (Emsley et al., 2000; Shimaoka et al., 2003) (see Figure 2B). However, the βFα7 loop and α7 helix differ between the C2a structures and Bb. The α7 helices differ by 27°–29° in orientation and are shifted approximately two-thirds of a helical turn toward the MIDAS site in C2a (Figure 2C). Superposition of C2a with closed and open α_2 and intermediate α_L-I domain structures (Shimaoka et al., 2003) shows no evident similarities in the backbone position of loop βFα7 and helix α7. Although the C2a α7 helix is positioned between the open and closed states of α_2 I domains, it differs from the intermediate position observed in the α_L I domain due to a tilt of helix α7 in C2a (Figure 2C).

Based on structural data and molecular dynamic simulations, Jin et al. (2004) suggest that the position of the α7 helix in I domains is stabilized by hydrophobic "ratchet" residues that occupy underlying hydrophobic pockets. For the α_2 and α_L I domains, respectively, 2 (315-VxxxxxL-321) and 3 (289-LxxFxxL-295) ratchet residues have been identified. Alignment indicates that C2a and Bb may have 2 hydrophobic ratchet residues, 419-LxxxxxL-425 in C2a and 430-VxxxxxL-436 in Bb, suggesting that the two VWA domains may occur in an open and closed conformation similar to those of the α_2 I domain. So far, only an open-like conformation for Bb has been observed, and the 2 ratchet residues, Val-430 and Leu-436, are positioned in hydrophobic pockets according to the activated, open I domains. The

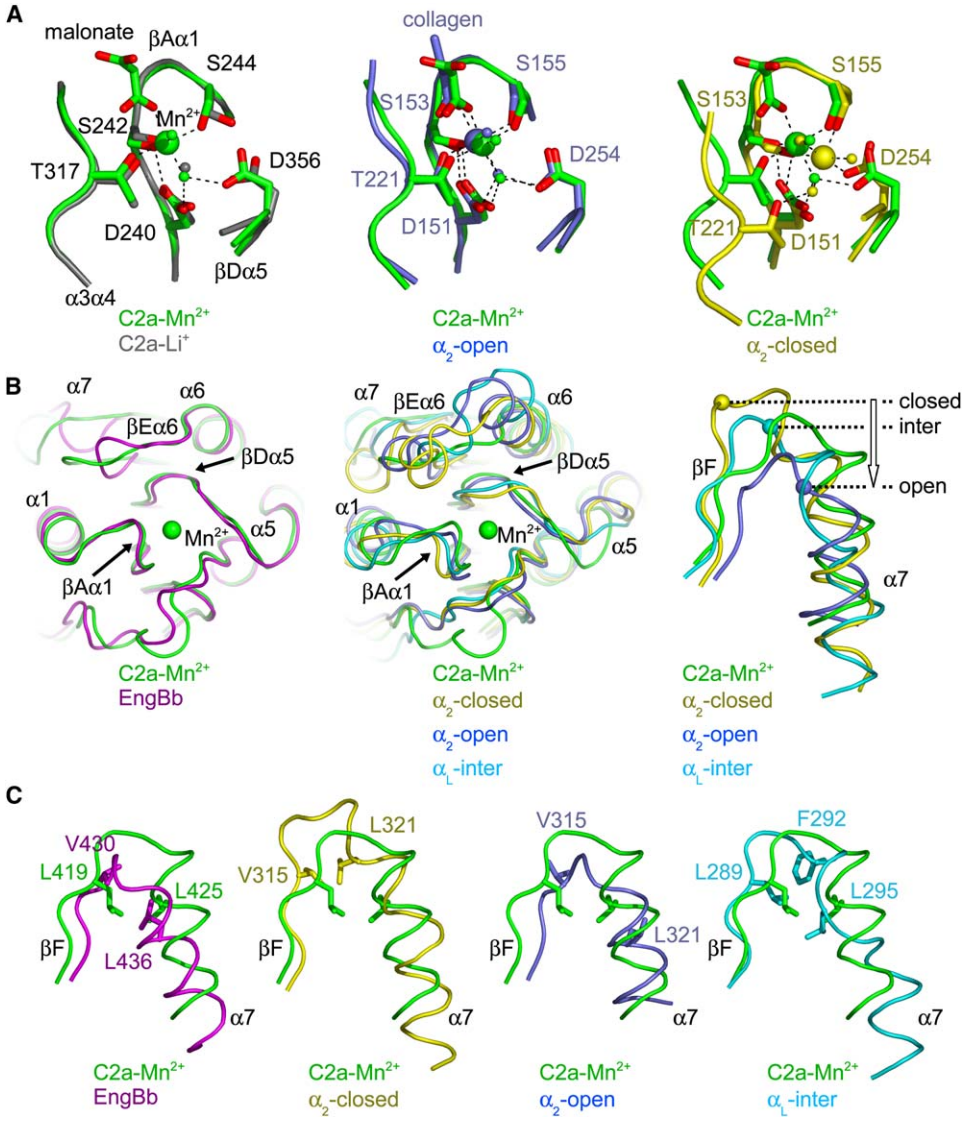

Figure 2. Activation State of the VWA Domain

(A) Left panel: the MIDAS motif of C2a as observed in the structures of C2a-Li^+ (gray) and C2a-Mn^{2+} (green). The MIDAS residues (residue number and loop names are as indicated), the pseudo ligand malonate, waters (small spheres), and Mn^{2+} (large sphere) are shown. Middle and right panels: the MIDAS motif of C2a-Mn^{2+} and the α_2-I domain in an open (1dzi, blue) and closed (1aox, yellow) conformations (Emsley et al., 1997, 2000).

(B) View of the VWA domain. Left panel: C2a-Mn^{2+} (green) and engineered open Bb (1rrk, magenta) (Ponnuraj et al., 2004); middle panel: C2a-Mn^{2+} (green), closed (1aox, yellow) and open (1dzi, blue) α_2 (Emsley et al., 1997, 2000), and intermediate (1mjn, light blue) α_L-I (Shimaoka et al., 2003) domains; and, right panel: coil representation of the strand βF and helix α7, colored as in the middle panel. The conformations of loops βAα1 and βDα5 and helix α1 transmitting structural changes between the MIDAS motif and helix α7 are indicated.

(C) Position of hydrophobic "ratchet" residues of loop βFα7 and helix α7, colored as in (B). From left to right: C2a-Mn^{2+} and engineered open Bb, C2a-Mn^{2+} and closed α_2, C2a-Mn^{2+} and open α_2, and C2a-Mn^{2+} and intermediate α_L.

situation in C2a, however, differs. The first ratchet residue of C2a, Leu-419, most resembles the situation observed for α_2 in the closed conformation and α_L in either the closed or intermediate conformation (Figure 2C). The second putative ratchet residue of C2a, Leu-425, is located at an uncommon position: it sits between the position that the second α_2 ratchet residue occupies in the closed and open conformation, and it overlaps with the position of the third α_L ratchet residue in the intermediate conformation (Figure 2C). These differences with Bb, α_2, and α_L are possibly due to differences in loop βEα6 (Figure 2B). This loop is 1 residue longer in C2a than in Bb and adopts a different conformation, with the side chain of Val-393 occluding the ratchet pocket (for the second ratchet residue in the open conformation), as observed in Bb, α_2, or α_L. In conclusion, C2a has 2 putative ratchet residues, and their positions correspond best with those of an intermediate conformation of the α7 helix.

C2a N Terminus

We expected the N terminus of C2a, which is formed upon proteolysis of C2 in the C4bC2 complex, to be unstructured. Surprisingly, however, the N-terminal

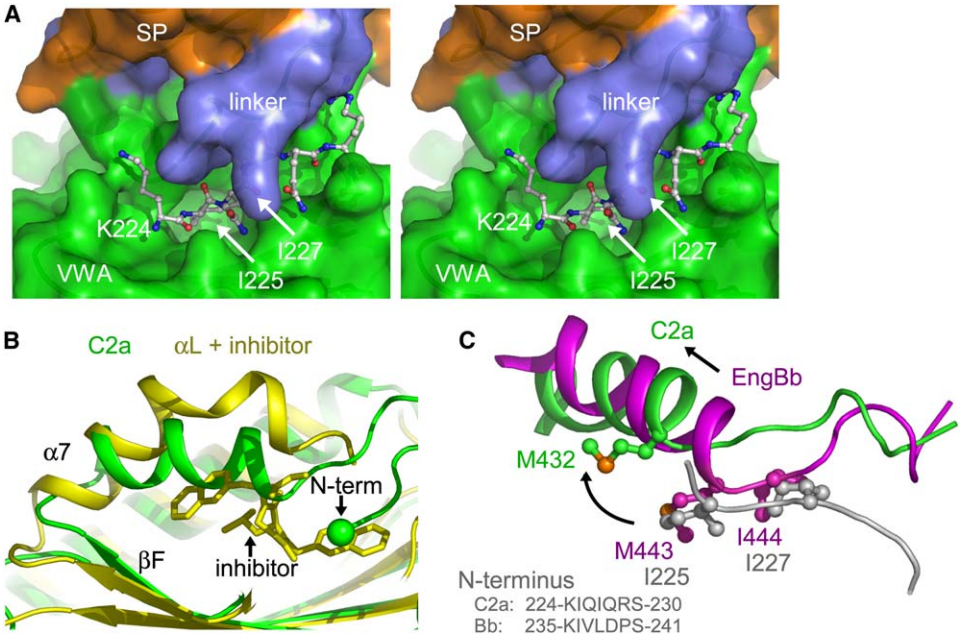

Figure 3. N-Terminal Residues of C2a

(A) Stereo figure showing the N-terminal residues (ball-and-stick) of C2a positioned in a crevice near the linker (blue) connecting the VWA (green) and SP (orange) domains. The C2a N terminus is anchored via Ile-225 and Ile-227, which are buried in underlying hydrophobic pockets.

(B) Overlay of C2a-Mn^{2+} (green) and the closed α_L-I domain (1xuo, yellow) in complex with a small-molecule antagonist (Wattanasin et al., 2005). The binding sites for the N-terminal segment in C2a and the antagonist partially overlap.

(C) Overlay of the N- and C-terminal regions of the VWA domain of C2a (green) and engineered Bb (1rrk, magenta) (Ponnuraj et al., 2004). In C2a, the N-terminal residues interact with α7, and Ile-225 and Ile-227 occupy hydrophobic pockets. In engineered Bb residues of the C-terminal end of α7 (Met-443 and Ile-444) occupy these hydrophobic pockets.

residues (224–231) are well ordered and positioned in a groove near the VWA-SP interface region. Strands βA and βD and the C-terminal end of the VWA domain form a crevice in which the N-terminal residues are bound via the side chains of Ile-225 and Ile-227, which are deeply buried in hydrophobic pockets (Figure 3A). Furthermore, the main chain of residues 225–227 forms a small, irregular parallel β sheet with residues 432–434 C-terminal of helix α7. Residues 228–231 form a loop that connects to the first strand (βA) of the VWA domain. Additional contacts of the N-terminal residues with the VWA-SP linker region involve a salt bridge, hydrogen bonds, and hydrophobic contacts. Thus, the N-terminal residues of C2a interact extensively with the VWA domain and VWA-SP interface.

The observed interactions of the C2a N-terminal segment with residues in the C-terminal end of the VWA domain are absent in the models of the isolated VWA domain of factor B (Bhattacharya et al., 2004) and engineered Bb (Ponnuraj et al., 2004) due to disorder and truncation of the N-terminal residues, respectively. The conformation of the N-terminal segment in C2a is, however, consistent with the observation made by Hinshelwood and Perkins (2000). Based on up-field methyl NMR spectra, these authors suggest that in Bb, and not in factor B or the isolated VWA domain, the N terminus 235-KIVLD-239 is structurally incorporated in the proximity of an aromatic residue. Indeed, the homologous residues in C2a (224-KIQIQ-228) are within 4–6 Å of 3 aromatic residues (Tyr-389, Phe-429, and Phe-267), which are identical or homologous aromatic residues in factor B. Furthermore, the structure of the N-terminally truncated Bb shows a similar crevice, which may harbor the N-terminal residues in full-length Bb. However, binding of the N terminus in this crevice requires the presence of the SP domain, because the N-terminal residues and helix α7 are disordered in the isolated VWA structure of factor B. The fragments C2a and Bb arise after binding of C2 and B, respectively, to their cofactors and subsequent proteolysis between the third CCP and the VWA domain. For proteolysis, the loop with the scissile bonds, Arg-223–Lys-224 of C2 and Arg-234–Lys-235 of B, must be exposed. In the structure of C2a, however, the main-chain atoms of Lys-224 are buried and inaccessible to the C1s or MASP-2 proteases. Thus, the N-terminal residues of C2a and Bb must adopt a conformation in the C4bC2 and C3bB complexes that is drastically different from the conformation observed in C2a.

The binding site for the N-terminal segment in C2a partially overlaps with the small-molecule antagonist-binding site observed in the α_L I domain (Crump et al., 2004; Kallen et al., 1999; Wattanasin et al., 2005) (see Figure 3B). Binding of antagonists locks the α_L I domains in an inactive, closed conformation of both the α7 helix and the MIDAS site. In contrast, in C2a we observe an intermediate-like conformation for helix α7 and an open conformation of the MIDAS site. This difference is perhaps correlated with the precise location of binding the antagonist versus binding the N terminus; i.e., the antagonists bind adjacent to the helix, whereas the N terminus binds at the C-terminal end of the helix (Figure 3B). Comparison of C2a and Bb indicates that binding of the N-terminal segment likely dislocates the α7 helix (see Figure 3C). A prominent aspect of binding

the N-terminal segment in C2a is the positioning of Ile-225 and Ile-227 in well-defined hydrophobic pockets. In engineered, truncated Bb, these two pockets are occupied by hydrophobic residues Met-443 and Ile-444 of the C-terminal end of helix α7. Thus, the position of the α7 helix in Bb is incompatible with binding of the N-terminal segment. We assume that in native, full-length Bb the N-terminal segment, with Ile-236 and Leu-238, will dislocate the α7 helix as in C2a (Figure 3C). The structure of C2a indicates that dislocation of the α7 helix by the N terminus causes rearrangements in the VWA-SP interface region.

Domain-Domain Interface

The VWA-SP interface area is significantly larger in C2a than in Bb: 1967 and 1920 Å^2 buried surface area in C2a-Li^+ and C2a-Mn^{2+}, respectively, versus 1320 Å^2 in Bb (computed by using domain boundaries as defined by Ponnuraj et al., [2004]). The linker region, residues 433–442, interacts intimately with both the VWA and SP domains. The contacts between the two domains involve numerous van der Waals interactions, hydrogen bonds, and three salt bridges. Three aspects contribute to the difference in buried surface area. First, the domain-domain orientations differ by 16°–21° in C2a and Bb and the α7 helices take on different positions. Consequently, the interface has a more compact arrangement in C2a (Figure 1C). Second, the contribution of the α7 helix to the buried surface area increases from 191 Å^2 in Bb to 286 and 271 Å^2 in C2a-Li^+ and C2a-Mn^{2+}, respectively. Third, in addition, in C2a, two N-linked glycans at asparagines 447 and 451 are located at or near the VWA-SP domain interface (Figure 1B; both glycosylation consensus sequences are conserved among the known C2 sequences). The glycan at Asn-447 contributes significantly (~250 Å^2) to the buried surface area in both C2a structures. The glycan at Asn-451 contributes another 60 Å^2 in the C2a-Li^+ model (this glycan was not modeled in C2a-Mn^{2+}). Carbohydrate units of the glycan at Asn-447 make multiple hydrogen bonds with residues of both the linker and VWA and SP domains. Hydrogen bonds are formed between the first GlcNAc unit and residues from the VWA α7 helix (Glu-430), the linker (Leu-433), and the first SP 3_{10} helix (Glu-456) and between the second GlcNAc unit with the N terminus (Lys-224), the VWA α7 helix (His-431), and the linker (Asp-434). To verify the role of these glycans, we made native C2, two single-glycan-deletion mutants (N447D and N451D), and one double-glycan-deletion mutant (N447D/N451D) that were tested for hemolytic activity. Compared to native C2, the N451D mutant has enhanced activity (149% ± 36%), indicating that this glycan is not required for activity. In contrast, the N447D mutant is almost hemolytic inactive (4.0% ± 0.1% residual activity). In the double mutant N447D/N451D, however, the activity slightly recovers to 22% ± 8%. This indicates that the N447 interface glycan plays an important, but not critical, role in C4b2a convertase stability or activity.

SP Domain

The catalytic residues, His-487, Asp-541, and Ser-659, of C2a are in an active conformation. The oxyanion-hole loop, Lys-656–Ser-659, adopts a conformation similar, but not identical, to that of mature trypsins and chymotrypsins (Figure 4A). As observed in the structure of Bb (Ponnuraj et al., 2004), one of the oxyanion-hole-forming peptide planes in C2a (between Lys-656 and Gly-657) is flipped by ~180° compared to trypsin. Although Arg-696 in loop 2 of C2a takes over the role of Ile-16, which induces oxyanion-hole formation in trypsin, this does not suffice to establish a fully formed oxyanion hole. In C2a, the carbonyl oxygen of Lys-656 points inward and makes a hydrogen bond with the catalytic serine hydroxyl, whereas in activated trypsin, the amide group of Gly-193 points inward to stabilize the oxyanion-reaction intermediate (Khan and James, 1998). In trypsin, the peptide plane is stabilized in a proper orientation by a hydrogen bond between Asn-143 of loop D and the carbonyl of Gln-192 (Figure 4A). Compared to trypsins and chymotrypsins, C2a and Bb have a very short loop D and a long loop 2. Nonetheless, a structural homolog of Asn-143 is not provided in either C2a or Bb. As suggested (Jing et al., 2000; Ponnuraj et al., 2004), the ill-formed oxyanion hole may explain the low proteolytic activity toward peptide substrates (Kam et al., 1987).

The substrate binding grooves in C2a and Bb differ significantly from trypsin due to large insertions and deletions in surface loops (Figure 4B; with substrate binding loops labeled according to Perona and Craik, [1997]). In comparison to trypsin, loops 2, 3, and C are respectively 15, 13, and 9 residues longer, and loops D and E are respectively 12 and 4 residues shorter in C2a. Notably, the extended loops 3 and C enclose the left side of the putative substrate-binding groove (Figure 4B). Thus, the ordinary S2- and S3-binding pockets appear to be absent in C2a and Bb. Differences between C2a and Bb occur primarily in the putative substrate-binding loop E and loop 2. Loop E is positioned near the interface region of the VWA and SP domains, and the observed differences may result from the differences in domain-domain orientation between C2a and Bb. Loop 2 is 7 residues longer in C2a than in Bb. This loop is disordered in all structures of C2a and Bb; respectively, 691-KNS-693 and 701-KNQ-703 are missing in all models. These residues are part of a conserved positively charged stretch (692–698 in C2a and 701–707 in Bb; these include arginines 696 in C2a and 705 in Bb, which interact with the oxyanion hole). This stretch may provide a specific electropositive patch for interactions with substrate C3. Other surface charges conserved between C2a and Bb are located within loops A, B, and C near the S1-binding pocket. As shown in Figure 4B, loops 2 and D on one side and loops A and B on the other side form a distinct binding groove, similar to the substrate-binding groove in trypsin. In contrast, the substrate-binding grooves in C2a and Bb are delineated by an obstruction formed by the extended loops 3 and C, which is likely to play a part in the high substrate specificity of C2a and Bb.

The SP domains in C2a and Bb are in near-active conformations. Hence, we may assume that the SP domains do not undergo large structural changes in cofactor binding (i.e., in the formation of C4b2a and C3bBb) and substrate C3 binding. Figure 4C represents a simple model of the enzyme-substrate complex. This model is obtained by placing C3 (Janssen et al., 2005) onto C2a, with the scissile loop oriented in a productive N to C

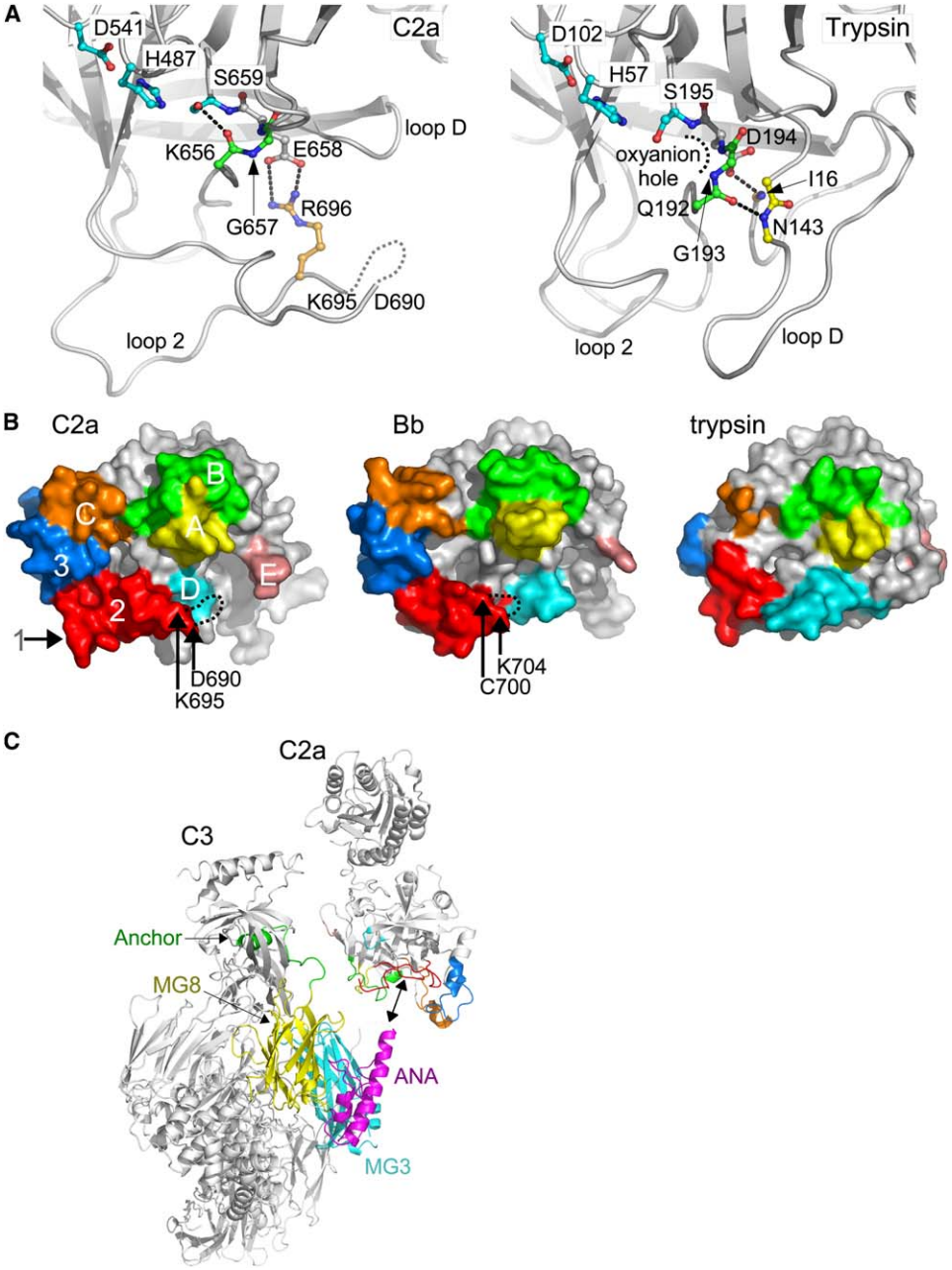

Figure 4. The SP Domain

(A) Catalytic center and oxyanion hole in C2a-Li^+ (left panel) and trypsin (1avw, right panel) (Song and Suh, 1998); the catalytic triad Asp-His-Ser (light blue), the oxyanion hole (green), and Arg-696 (orange) in C2a, replacing the N-terminal Ile-16 in trypsin, are indicated. In trypsin the main chain of Asn-143 (yellow) forms a hydrogen bond with the main chain of 192–193. A similar interaction is absent in C2a. Instead, the peptide plane of 656–657 is flipped and makes a hydrogen bond with the catalytic serine.

(B) Surface representation of the putative substrate-binding grooves; C2a-Li^+ (left panel), Bb (1rrk, middle panel) (Ponnuraj et al., 2004), and trypsin (1avw, right panel) (Song and Suh, 1998) are shown. Surface loops 1 (gray), 2 (red), 3 (blue), A (yellow), B (green), C (orange), D (light blue), and E (pink) are highlighted.

(C) Hypothetical model of C2a placed onto C3 (2a73 [Janssen et al., 2005]); the SP domain of C2a (substrate binding loops are colored as in [B]) and substrate C3 (the flexible scissile loop is indicated by a dotted line) are shown. Domains of C3 are labeled as defined in Janssen et al. [2005].

direction in the primary substrate-binding groove. In the structures of human and bovine C3, the scissile loop is disordered and exposed to the solvent (Fredslund et al., 2006; Janssen et al., 2005); in human C3, 9 residues of the scissile loop (720–728) are absent in the model, and the Cα atoms of residues 719 and 729 are 11 Å apart in the structure of C3. The simple enzyme-substrate model identifies putative interactions between C2a, or Bb, and C3. Loops 2, 3, and C on the SP domain likely interact with the anaphylatoxin domain of C3. These extended loops may increase the contact area between the two proteins by positioning themselves around the protruding anaphylatoxin domain. Loops A and B possibly contact the residues following the

scissile bond and macroglobulin (MG)3 domain. Several complementary charges are present, suggesting a significant contribution from electrostatic interactions. Putative interactions of the anchor and MG8 domain of C3 may stabilize the partially disordered loop 2, potentially aiding in the formation of a mature oxyanion hole. These latter interactions support a substrate-induced activation mechanism of the SP domain proposed by Ponnuraj et al., (2004). Based on the observed VWA-SP orientation, the VWA domain is located in this enzyme-substrate model close to the C345C domain of C3. It may thus bridge interactions between the substrate C3 and the ligand, C4b or C3b, which is thought to bind at the MIDAS motif on the VWA domain. Of course, given the size of the molecules, we may expect additional interaction sites that may be important in the substrate affinity and specificity of the C3 convertases. Modeling these interactions requires a structure of either C3b or C4b. Nonetheless, the enzyme-substrate model presented here identifies a series of potential interaction sites that will help direct mutagenesis studies.

Concluding Remarks

The two structures of C2a give insights into the possible roles of the VWA domain in convertase formation and indicate potential primary and secondary interaction sites between the SP domain and substrate C3. The VWA domain of C2a does not require its ligand, C4b, to maintain an open conformation of the MIDAS motif. The open MIDAS conformation observed in unliganded C2a-Li^+ and pseudo liganded C2a-Mn^{2+} possibly serves to enhance the affinity for C4b. The N-terminal residues of C2a are buried in the VWA domain, possibly stabilizing the observed intermediate conformation of the VWA-α7 helix. The observed structure implies that the N-terminal residues undergo a conformational change from exposed and accessible to proteases in the C4bC2 complex to inaccessible in C2a. An extensive contact area is observed between the VWA and SP domains of C2a. Glycan N447 contributes significantly to the domain-domain interface. This glycan is important, but not critical, for hemolytic activity. As was previously observed in the structure of engineered Bb, the open VWA domain in C2a does not suffice to induce a fully active conformation of the SP domain. The proposed substrate-induced activation mechanism, forming a fully active oxyanion hole upon C3 binding, possibly involves loop 2 of the SP domain. In a simple substrate-enzyme (C3-C2a and C3-Bb) model, the negative charges of the anchor region and/or MG8 of C3 possibly interact with the positive charges of the extended, and unique, loop 2 of C2a and Bb. Extensions of substrate binding loops 2, 3, and C possibly serve to enhance the contact area by enveloping the protruding anaphylatoxin domain in C3, hence contributing to substrate affinity and specificity.

Experimental Procedures

Cloning and Expression of Recombinant C2a and C2

The cDNA coding for human C2a was amplified by PCR from I.M.A.G.E. clone 2191586. Forward primer C2afor (5′-GGATCCGCTC CCTCCTG-3′) introduced a BamHI restriction site. Reverse primer C2rev (5′-GCGGCCGCGAGGGGTAAAAAATTCAGGA-3′), which anneals to the 3′ untranslated region, introduced a NotI restriction site. The PCR product was cloned in the pCR4-TOPO vector (Invitrogen) and sequenced. Next, C2a was ligated as a BamHI-NotI fragment into a pNUT expression vector (Palmiter et al., 1987) that encodes the secretion signal peptide of human von Willebrand factor followed by a hexa-histidine tag. This construct was used for transfection of BHK cells according to the DNA-calcium phosphate method (Graham and van der Eb, 1973). Colonies were selected on 100 μM methotrexate. For identification of highly expressing clones, expression medium was diluted 50- to 100-fold in coating buffer (50 mM sodium carbonate, 0.02% sodium azide [pH 9.6]), coated in 96-well plates, and probed with anti-polyhistidine monoclonal antibody his-1 (Sigma) followed by horseradish peroxidase-coupled rabbit-anti-mouse antibodies (DAKO). For large-scale production, cells were cultured in a cell factory (Nunc) with Ultroser G (ITK Diagnostics) as serum replacement. Expression medium was stored at −20°C until further use.

For construction of the human C2 expression vector, a PCR was performed with forward primer C2for (5′-GCAGGATCCGCTCCC TCCTGCCCT-3′) and reverse primer C2rev. The PCR product was cloned in pCR4-TOPO and sequenced. This plasmid served as a template for the generation of glycosylation mutants C2-N447D and C2-N451D and the double glycosylation mutant C2-N447D/N451D. Mutagenesis was achieved by an "in house" variation of the QuikChange method. In the case of mutant C2-N447D, a PCR was performed with limiting amounts (6 pmol) of forward mutagenesis primer N447D (5′-GGGGTGGGGGACATGTCAGC-3′) and primer C2rev with 100 ng (~25 fmol) pCR4-C2 template and 1.7 U Pfu Turbo DNA polymerase (Stratagene). After a few PCR cycles, both primers are exhausted. The PCR product then provides two complementary mega-primers that, in a QuikChange-like reaction, generate full-length mutated copies of the template vector. After completion of the reaction, template vector was destroyed by incubation with DpnI restriction enzyme (NewEngland Biolabs) for 2 hr at 37°C, and 5 μl of the reaction product was transformed into Top10 cells. For the construction of mutant C2-N451D, a similar PCR reaction was performed with primer C2for and reverse mutagenesis primer N451Drev (5′-CAGAGGCGTCTGCTGACATG-3′). The double mutant was constructed by using mutation primers N447Dfor and N451Drev. Introduction of the respective mutations was confirmed by sequencing. C2 and C2 mutants were ligated in a modified pTT3 expression vector (Durocher et al., 2002) encoding a cystatin secretion signal peptide (Barash et al., 2002) followed by a hexa-histidine tag. Suspensions growing HEK293-EBNA-1 (Epstein-Barr virus nuclear antigen 1) cells were transfected with polyethyleneimine (Durocher et al., 2002), and recombinant mutant C2 was transiently expressed at low serum concentration (~0.1% fetal calf serum). Expression medium containing C2 was harvested 96 hr after transfection and stored at −20°C until further use.

Hemolytic Assay

Hemolytic activity of recombinant C2 was assessed by a C2-dependent hemolytic assay, by using C2-deficient guinea pig serum as a complement source. The method was similar to that previously described for a C1q-dependent hemolytic assay (Roos et al., 2001). In brief, 1.10^7 antibody-coated sheep erythrocytes were incubated with 100-fold diluted C2-deficient serum in the presence or absence of culture supernatant containing human recombinant C2 or C2a, normal human serum, or mock culture supernatant, in various dilutions, for 1 hr at 37°C. The assay was performed with dextrose gelatin Veronal buffer^{2+} ($DGVB^{2+}$) as a buffer in a final volume of 200 μl. $DGVB^{2+}$ consists of 0.05% gelatin, 167 mM glucose, 0.15 mM $CaCl_2$, 0.5 mM $MgCl_2$ in veronal-buffered saline (1.8 mM Na-5,5-diethylbarbital, 0.2 mM 5,5-diethylbarbituric acid, 145 mM NaCl). After addition of 1.5 ml phosphate-buffered saline and centrifugation, hemolysis was assessed by measuring OD at 414 nm. C2 hemolytic activity was calculated as a z value, as described (Roos et al., 2001), followed by calculation of hemolytic activity per milliliter and normalization for the concentration of C2 as determined by specific ELISA. The relative hemolytic activity of mutant C2 was calculated as a percentage of hemolytic activity of wild-type C2.

Purification of C2a

C2a expression medium was concentrated 10-fold by using a Quickstand bench top concentrator (GE Health Care) with a 10 kDa

molecular weight cut off, and the pH of the medium was adjusted to 8.0. Next, C2a was purified from concentrated medium by using a Hi-Trap-chelating HP column (Amersham) charged with Ni^{2+}. After loading, the column was extensively washed with buffer containing 20 mM Tris, 300 mM NaCl (pH 8). Nonspecifically bound proteins were eluted with 15 mM imidazole in the same buffer. Next, C2a was eluted at an imidazole concentration of 100 mM. Peak fractions were analyzed by SDS-PAGE and Western blotting with antibodies directed against the His-tag. The N-terminal sequence was analyzed on an automated protein sequencer from Perkin Elmer Applied Biosystems 476A, confirming the presence of the expected amino acids HHHHHHGSKI.

Crystallization and Diffraction Data Collection

For crystallization, purified C2a was dialyzed against a solution containing 20 mM Tris, 50 mM NaCl (pH 7.5) and was concentrated to 15 mg/ml. Crystallization experiments were performed at 20°C by using the hanging-drop vapor-diffusion method and a 1:1 ratio of protein and reservoir solution. Initial crystals of poor quality were obtained with reservoir solution consisting of 35% w/v PEG 1000 and 0.1 M malonate-imidazole boric acid buffer, made by mixing 0.1 M sodium malonate, 0.1 M imidazol, and 0.1 M boric acid in a 2:3:3 ratio, at pH 7.0. A subsequent screen for additives identified two conditions that produced crystals suitable for data collection. In the presence of 20 mM LiCl, triangular crystals with dimensions of 0.08 × 0.06 × 0.02 mm appeared after 4–5 days. We refer to these crystals as C2a-Li^+. For data collection, a C2a-Li^+ crystal was passed through a 2 μl drop of reservoir solution and rapidly frozen by immersion in liquid nitrogen. In the presence of xylitol at a concentration of 3%, w/v crystals of 0.1 × 0.1 × 0.1 mm appeared after 5 months. These crystals were soaked for 24 hr in a 2 μl drop of reservoir solution containing 20 mM NaCl and 10 mM $MnCl_2$ and were then flash cooled in liquid nitrogen. We refer to these crystals as C2a-Mn^{2+}. Diffraction data up to a resolution of 2.7 Å for C2a-Li^+ and 2.1 Å for C2a-Mn^{2+} were collected at ESRF beam-lines ID14-EH2 and ID14-EH4 in Grenoble, France. The data were indexed and integrated with MOSFLM (Leslie, 2006) and were scaled with SCALA (CCP4, 1994). Data statistics are given in Table 1.

Structure Determination and Refinement

The structure of C2a was determined by molecular replacement with Phaser (Storoni et al., 2004). As search models, we used the coordinates of Protein Data Bank entries 1DLE (Jing et al., 2000) and 1Q0P (Bhattacharya et al., 2004), representing the SP and VWA domains, respectively, of factor B. Sequence identities between C2 and factor B are 39% for these domains. Phaser yielded a clear answer, where attempts with other programs had failed, placing first the SP domain and subsequently the VWA domain. Reversing the order, i.e., starting with the smaller VWA domain, yielded the same solution.

The model of C2a-Li^+ was iteratively built by using the program O (Jones et al., 1991) and was refined to near completion with CNS (Brunger et al., 1998) and REFMAC (Winn et al., 2001). Subsequently, higher-resolution diffraction data of C2a soaked with $MnCl_2$ were obtained, and its structure was solved and refined, yielding a more complete model. The C2a-Mn^{2+} model was then used to finalize the model of C2a-Li^+. The final R and R_{free} factors were 0.21/0.29 for all data out to 2.7 Å resolution for C2a-Li^+ and 0.19/0.24 for all data to 2.1 Å resolution for C2a-Mn^{2+}. Both models display good geometry (see Table 1). The final model for C2a-Li^+ consists of 497 protein residues, 11 glycan units, and 38 water molecules. Due to poor electron density, residues 395–397, residues 408–413, and residues 691–694 were excluded from the model. The final model for C2a-Mn^{2+} consists of 502 protein residues, 7 glycan units, 133 water molecules, and 1 Mn^{2+} ion. Residues 687–693 are missing due to unclear electron density.

Acknowledgments

We thank the ID14 beam-line scientists at the European Synchrotron Radiation Facility (EMBL/ESRF) in Grenoble, France for their help with data collection. We thank Randy J. Read for solving the molecular replacement problem in minutes at the European Molecular Biology Organization course "Automated Macromolecular Structure Solution" in Amsterdam. We acknowledge Shizuko Tsuji for her help with expression of C2a in BHK cells. Danielle J. van Gijlswijk-Janssen and Nicole Schlagwein (LUMC, Leiden) are acknowledged for technical assistance. We are indebted to one of the referees for very helpful criticisms. This work was supported by "Pionier Programme" grant No. 700.99.402 (P.G.) of the Council for Chemical Sciences of the Netherlands Organization for Scientific Research (NWO-CW) and the Dutch Kidney Foundation (A.R.).

Received: March 17, 2006
Revised: August 30, 2006
Accepted: August 30, 2006
Published: October 10, 2006

References

Barash, S., Wang, W., and Shi, Y. (2002). Human secretory signal peptide description by hidden Markov model and generation of a strong artificial signal peptide for secreted protein expression. Biochem. Biophys. Res. Commun. *294*, 835–842.

Bentley, D.R. (1986). Primary structure of human complement component C2. Homology to two unrelated protein families. Biochem. J. *239*, 339–345.

Bhattacharya, A.A., Lupher, M.L., Jr., Staunton, D.E., and Liddington, R.C. (2004). Crystal structure of the A domain from complement factor B reveals an integrin-like open conformation. Structure *12*, 371–378.

Bode, W. (1979). The transition of bovine trypsinogen to a trypsin-like state upon strong ligand binding. II. The binding of the pancreatic trypsin inhibitor and of isoleucine-valine and of sequentially related peptides to trypsinogen and to p-guanidinobenzoate-trypsinogen. J. Mol. Biol. *127*, 357–374.

Brunger, A.T., Adams, P.D., Clore, G.M., DeLano, W.L., Gros, P., Grosse-Kunstleve, R.W., Jiang, J.S., Kuszewski, J., Nilges, M., Pannu, N.S., et al. (1998). Crystallography & NMR system: a new software suite for macromolecular structure determination. Acta Crystallogr. D Biol. Crystallogr. *54*, 905–921.

CCP4 (Collaborative Computational Project, Number 4) (1994). The CCP4 suite: programs for protein crystallography. Acta Crystallogr. D Biol. Crystallogr. *50*, 760–763.

Crump, M.P., Ceska, T.A., Spyracopoulos, L., Henry, A., Archibald, S.C., Alexander, R., Taylor, R.J., Findlow, S.C., O'Connell, J., Robinson, M.K., and Shock, A. (2004). Structure of an allosteric inhibitor of LFA-1 bound to the I-domain studied by crystallography, NMR, and calorimetry. Biochemistry *43*, 2394–2404.

Durocher, Y., Perret, S., and Kamen, A. (2002). High-level and high-throughput recombinant protein production by transient transfection of suspension-growing human 293-EBNA1 cells. Nucleic Acids Res. *30*, E9.

Emsley, J., King, S.L., Bergelson, J.M., and Liddington, R.C. (1997). Crystal structure of the I domain from integrin α2β1. J. Biol. Chem. *272*, 28512–28517.

Emsley, J., Knight, C.G., Farndale, R.W., Barnes, M.J., and Liddington, R.C. (2000). Structural basis of collagen recognition by integrin α2β1. Cell *101*, 47–56.

Fredslund, F., Jenner, L., Husted, L.B., Nyborg, J., Andersen, G.R., and Sottrup-Jensen, L. (2006). The structure of bovine complement component 3 reveals the basis for thioester function. J. Mol. Biol. *361*, 115–127.

Graham, F.L., and van der Eb, A.J. (1973). A new technique for the assay of infectivity of human adenovirus 5 DNA. Virology *52*, 456–467.

Hinshelwood, J., and Perkins, S.J. (2000). Conformational changes during the assembly of factor B from its domains by (1)H NMR spectroscopy and molecular modelling: their relevance to the regulation of factor B activity. J. Mol. Biol. *301*, 1267–1285.

Horiuchi, T., Macon, K.J., Engler, J.A., and Volanakis, J.E. (1991). Site-directed mutagenesis of the region around Cys-241 of complement component C2. Evidence for a C4b binding site. J. Immunol. *147*, 584–589.

Janssen, B.J., Huizinga, E.G., Raaijmakers, H.C., Roos, A., Daha, M.R., Nilsson-Ekdahl, K., Nilsson, B., and Gros, P. (2005). Structures

of complement component C3 provide insights into the function and evolution of immunity. Nature *437*, 505–511.

Jin, M., Andricioaei, I., and Springer, T.A. (2004). Conversion between three conformational states of integrin I domains with a C-terminal pull spring studied with molecular dynamics. Structure *12*, 2137–2147.

Jing, H., Xu, Y., Carson, M., Moore, D., Macon, K.J., Volanakis, J.E., and Narayana, S.V. (2000). New structural motifs on the chymotrypsin fold and their potential roles in complement factor B. EMBO J. *19*, 164–173.

Jones, T.A., Zou, J.Y., Cowan, S.W., and Kjeldgaard. (1991). Improved methods for building protein models in electron density maps and the location of errors in these models. Acta Crystallogr. A *47* (Pt. 2), 110–119.

Kallen, J., Welzenbach, K., Ramage, P., Geyl, D., Kriwacki, R., Legge, G., Cottens, S., Weitz-Schmidt, G., and Hommel, U. (1999). Structural basis for LFA-1 inhibition upon lovastatin binding to the CD11a I-domain. J. Mol. Biol. *292*, 1–9.

Kam, C.M., McRae, B.J., Harper, J.W., Niemann, M.A., Volanakis, J.E., and Powers, J.C. (1987). Human complement proteins D, C2, and B. Active site mapping with peptide thioester substrates. J. Biol. Chem. *262*, 3444–3451.

Kerr, M.A. (1980). The human complement system: assembly of the classical pathway C3 convertase. Biochem. J. *189*, 173–181.

Kerr, M.A., and Parkes, C. (1984). The effects of iodine and thiol-blocking reagents on complement component C2 and on the assembly of the classical-pathway C3 convertase. Biochem. J. *219*, 391–399.

Khan, A.R., and James, M.N. (1998). Molecular mechanisms for the conversion of zymogens to active proteolytic enzymes. Protein Sci. *7*, 815–836.

Leslie, A.G. (2006). The integration of macromolecular diffraction data. Acta Crystallogr. D Biol. Crystallogr. *62*, 48–57.

Murshudov, G.N., Vagin, A.A., and Dodson, E.J. (1997). Refinement of macromolecular structures by the maximum-likelihood method. Acta Crystallogr. D Biol. Crystallogr. *53*, 240–255.

Palmiter, R.D., Behringer, R.R., Quaife, C.J., Maxwell, F., Maxwell, I.H., and Brinster, R.L. (1987). Cell lineage ablation in transgenic mice by cell-specific expression of a toxin gene. Cell *50*, 435–443.

Pangburn, M.K., and Muller-Eberhard, H.J. (1986). The C3 convertase of the alternative pathway of human complement. Enzymic properties of the bimolecular proteinase. Biochem. J. *235*, 723–730.

Perona, J.J., and Craik, C.S. (1997). Evolutionary divergence of substrate specificity within the chymotrypsin-like serine protease fold. J. Biol. Chem. *272*, 29987–29990.

Ponnuraj, K., Xu, Y., Macon, K., Moore, D., Volanakis, J.E., and Narayana, S.V. (2004). Structural analysis of engineered Bb fragment of complement factor B: insights into the activation mechanism of the alternative pathway C3-convertase. Mol. Cell *14*, 17–28.

Rawal, N., and Pangburn, M.K. (2001). Structure/function of C5 convertases of complement. Int. Immunopharmacol. *1*, 415–422.

Roos, A., Nauta, A.J., Broers, D., Faber-Krol, M.C., Trouw, L.A., Drijfhout, J.W., and Daha, M.R. (2001). Specific inhibition of the classical complement pathway by C1q-binding peptides. J. Immunol. *167*, 7052–7059.

Shimaoka, M., Xiao, T., Liu, J.H., Yang, Y., Dong, Y., Jun, C.D., McCormack, A., Zhang, R., Joachimiak, A., Takagi, J., et al. (2003). Structures of the α L I domain and its complex with ICAM-1 reveal a shape-shifting pathway for integrin regulation. Cell *112*, 99–111.

Song, H.K., and Suh, S.W. (1998). Kunitz-type soybean trypsin inhibitor revisited: refined structure of its complex with porcine trypsin reveals an insight into the interaction between a homologous inhibitor from *Erythrina caffra* and tissue-type plasminogen activator. J. Mol. Biol. *275*, 347–363.

Storoni, L.C., McCoy, A.J., and Read, R.J. (2004). Likelihood-enhanced fast rotation functions. Acta Crystallogr. D Biol. Crystallogr. *60*, 432–438.

Tomana, M., Niemann, M., Garner, C., and Volanakis, J.E. (1985). Carbohydrate composition of the second, third and fifth components and factors B and D of human complement. Mol. Immunol. *22*, 107–111.

Walport, M.J. (2001a). Complement. First of two parts. N. Engl. J. Med. *344*, 1058–1066.

Walport, M.J. (2001b). Complement. Second of two parts. N. Engl. J. Med. *344*, 1140–1144.

Wattanasin, S., Kallen, J., Myers, S., Guo, Q., Sabio, M., Ehrhardt, C., Albert, R., Hommel, U., Weckbecker, G., Welzenbach, K., and Weitz-Schmidt, G. (2005). 1,4-Diazepane-2,5-diones as novel inhibitors of LFA-1. Bioorg. Med. Chem. Lett. *15*, 1217–1220.

Winn, M.D., Isupov, M.N., and Murshudov, G.N. (2001). Use of TLS parameters to model anisotropic displacements in macromolecular refinement. Acta Crystallogr. D Biol. Crystallogr. *57*, 122–133.

Accession Numbers

Coordinates and structure factors are available in the Protein Data Bank under accession codes 2I6Q (C2a-Mn^{2+}) and 2I6S (C2a-Li^{+}).